# Thermal transport in twisted few-layer graphene*

Min-Hua Wang(王敏华), Yue-E Xie(谢月娥), and Yuan-Ping Chen(陈元平)†

*Laboratory for Quantum Engineering and Micro-Nano Energy Technology, Xiangtan University, Xiangtan* 411105, *China*

(Received 7 May 2017; revised manuscript received 23 July 2017; published online 30 September 2017)

Twisted graphene possesses unique electronic properties and applications, which have been studied extensively. Recently, the phonon properties of twisted graphene have received a great deal of attention. To the best of our knowledge, thermal transports in twisted graphene have been investigated little to date. Here, we study perpendicular and parallel transports in twisted few-layer graphene (T-FLG). It is found that perpendicular and parallel transports are both sensitive to the rotation angle $\theta$ between layers. When $\theta$ increases from 0° to 60°, perpendicular thermal conductivity $\kappa_\perp$ first decreases and then increases, and the transition angle is $\theta = 30°$. For the parallel transport, the relation between thermal conductivity $\kappa_\parallel$ and $\theta$ is complicated, because intra-layer thermal transport is more sensitive to the edge of layer than their stacking forms. However, the dependence of interlayer scattering on $\theta$ is similar to that of $\kappa_\perp$. In addition, the effect of layer number on the thermal transport is discussed. Our results may provide references for designing the devices of thermal insulation and thermal management based on graphene.

**Keywords:** twisted graphene, thermal transport, rotation angle, thermal conductivity

**PACS:** 63.22.Rc,63.20.kg,74.25.fc,65.80.Ck **DOI:** 10.1088/1674-1056/26/11/116503

## 1. Introduction

Graphene, a monolayer carbon sheet, possesses many excellent properties, such as high electric conductivity,[1–4] high thermal conductivity,[5–7] and high stability,[8,9] which results in extensive applications in various fields. By stacking graphene, two- or few-layer graphene can be formed. Beside the conventional AA and AB stacking graphene, different stacking sequences can result in various Moire patterns between layers.[10–12] In experiment, these twisted few-layer graphenes (T-FLGs) have been synthesized by using the chemical vapor deposition (CVD), mechanical exfoliation or growth on the carbon terminated SiC surfaces.[13–15] Although the interlayer interactions are weak Van der Waals force, the T-FLG shows completely different electronic properties from those of AA and AB stacking graphene structures, and their properties are strongly dependent on the rotation angle $\theta$. For example, Bstristzer and MacDonald studied the electronic structure of a twisted bilayer graphene, and found that in the continuum Dirac model, the Moire pattern periodicity leads to Moire Bloch bands;[16] Li *et al.* demonstrated that a rotation between graphene layers can generate Van Hove singularities, which can be brought arbitrarily close to the Fermi energy by varying the angle of rotation;[17] Dos Santos *et al.* also found that a significant reduction of Fermi velocity occurs in twisted graphene. Moreover, unlike the case of the AB stacked bilayer, a potential difference between layers does not open a gap in the spectrum.[18]

Recently, phonon properties of T-FLG have received attention gradually. Several experimental Raman studies found a series of phonon peaks in different energy regions, which is absent in the few-layer graphene without twist.[19,20] Cocemasov *et al.* found that the twisted bilayer graphene leads to the emergence of new phonon branches, termed entangled phonons.[21] Nika *et al.* found that the phonon specific heat has an intriguing dependence on the rotation angle $\theta$ in twisted bilayer graphene, which is particularly pronounced at low temperature.[22] These studies indicate that the twisted graphene structures have unique thermal properties. To the best of our knowledge, however, thermal transports in these twist graphenes have been reported little. Therefore, it is natural to ask what is the effect of twist on the thermal transport in few-layer graphene.

In this paper, we investigate the thermal transport properties of T-FLG, by using molecular dynamics (MD) simulations. Thermal transports in the parallel and perpendicular directions are considered, respectively. Our results show that perpendicular and parallel thermal conductivities $\kappa_\perp$ and $\kappa_\parallel$ are both strongly dependent on rotation angle $\theta$, and $\theta = 30°$ is a transition angle. Underlying mechanisms for the unique phenomenon are explained by out-of-plane phonon density of states (PDOS) and interlayer interaction energy.

## 2. Model and simulation method

Figures 1(a) and 1(b) show the simplest models for perpendicular and parallel transport in T-FLGs, respectively. Figure 1(a) is a three-layer structure, where hot and cold heat baths are placed on the top and bottom layers, respectively. Figure 1(b) shows a bilayer graphene where the hot and cold

*Project supported by the National Natural Science Foundation of China (Grant Nos. 51376005 and 11474243).

†Corresponding author. E-mail: chenyp@xtu.edu.cn

© 2017 Chinese Physical Society and IOP Publishing Ltd 

baths are located on the left and right terminals, respectively. The stacking forms of the T-FLGs can be tuned by rotating one of the graphene layers. Figure 1(c) shows an initial twisted bilayer graphene, which is in fact an AB stacking structure with a rotation angle $\theta = 0°$. The red dot in the red circle is denoted as a rotation center. When the top layer of graphene rotates clockwise, various twisted structures with different Moire patterns can be formed to be dependent on $\theta$. Figure 1(d) presents twisted structures with $\theta = 0°$, 15°, 30°, 45°, and 60°, respectively. One can note that the rotating period is 60°, in other words, the structure with $60° + \theta$ is the same as the structure with $\theta$, while $\theta = 60°$ corresponds to an AA stacking bilayer graphene. In the $\theta = 30°$ structure, the zigzag edges of the top layer align with the armchair edges of the bottom layer. While the patterns of the structures with $\theta = 15°$ and 45° are more complicated. For the perpendicular transport, the sizes of all graphene layers are fixed at width $W = 6.31$ nm and length $L = 6.24$ nm. For the parallel transport, the width and length of graphene layer are $W = 5.02$ nm, and $L = 13.01$ nm. To study the effect of twist on the thermal transport in T-FLG, twisted structures with more than 2 and 3 layers are considered. In these structures, the stacking form between even layers is AA as well as that between odd layers, while the stacking between even and odd layers can be twisted by a rotation angle $\theta$ as shown in Figs. 1(e) and 1(f).

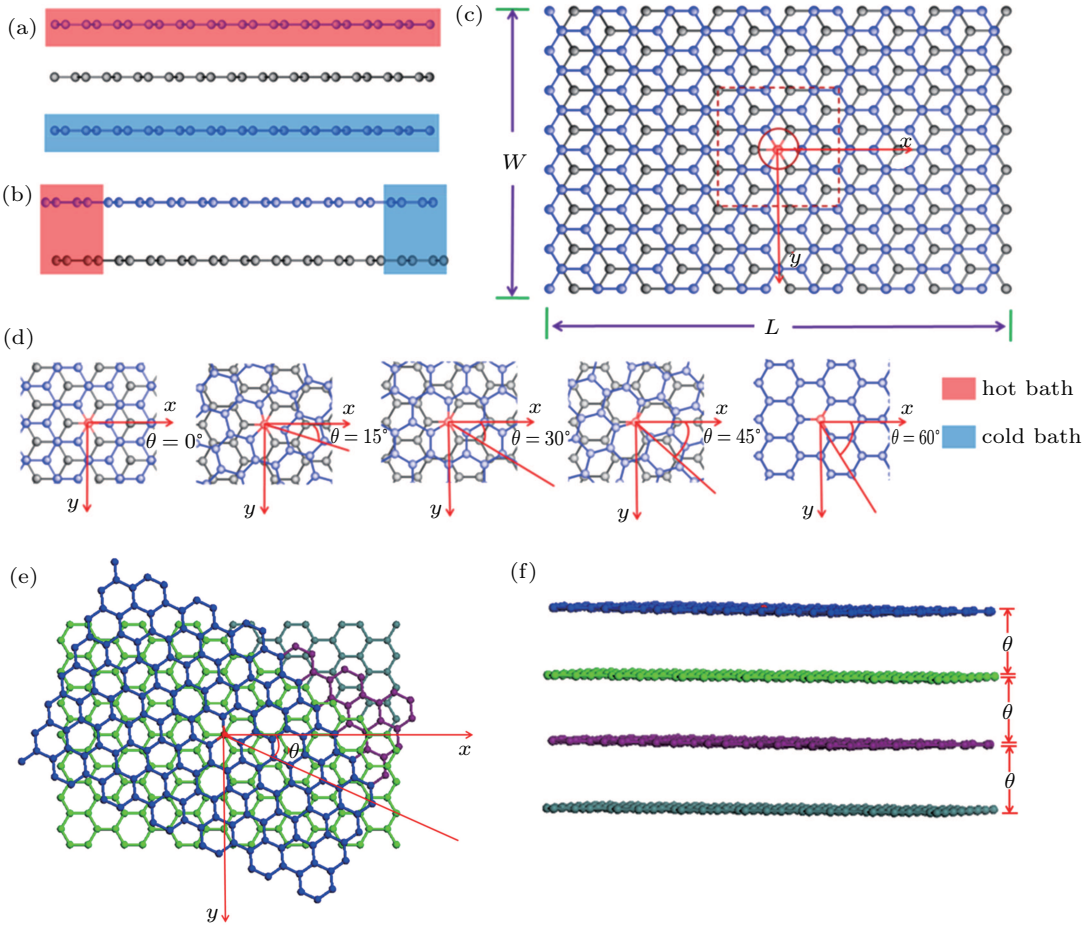



**Fig. 1.** (color online) Schematic views of T-FLGs. (a) Simplest model for perpendicular transport in twisted three-layer graphene. The red and blue regions represent hot and cold heat baths, respectively. (b) Simplest model for parallel transport in twisted bilayer graphene. (c) An initial twisted bilayer graphene with a size of $W \times L$, which is an AB stacking bilayer graphene with rotation angle $\theta = 0°$. The red dot represents the rotation center. Other twisted graphenes can be formed by clockwise rotating the top layer. (d) Twisted bilayer graphene structures with $\theta = 0°$, 15°, 30°, 45°, and 60°, respectively. (e) Top view of a T-FLG with a rotation angle $\theta$. Stacking form between even (or odd) layers is AA, while $\theta$ is the rotation angle between even and odd layers. (f) The side view of a T-FLG with a rotation angle $\theta$.

Thermal transport of T-FLG is calculated by MD method. All MD simulations here are performed by using the LAMMPS package.[23,24] An optimized Tersoff potential [25,26] is used to describe the interactions between intralayer carbon atoms. The 12-6 Lennard–Jones (LJ) potential is adopted to describe the interlayer van der Waals (VDWs) interactions:[27]

$$\Phi_{ij}(r) = 4\varepsilon_{ij}\left[\left(\frac{\sigma_{ij}}{r}\right)^{12} - \left(\frac{\sigma_{ij}}{r}\right)^{6}\right], \quad (1)$$

where $r$ represents the distance between two atoms, $\varepsilon$ is the energy that reflects their interaction strength, and $\sigma$ denotes the zero-across distance of the potential. The parameters of

the LJ potential are cited from Refs. [28] and [29]. The cutoff distance of VDWs force is chosen to be 10 Å. We first relax all the twisted structures under the canonical ensemble (NVT) conditions for 50 picoseconds (ps), in time steps of 0.5 femtoseconds (fs). The heat baths are Nosé–Hoover thermostats, and the temperatures of hot and cold baths are $T_0 + \Delta T$ and $T_0 - \Delta T$, respectively, to achieve a temperature gradient. $T_0$ is set to be environment temperature (300 K) and the temperature drop is set to be $\Delta T = 30$ K. In order to avoid the graphene moving in the simulations, we use fixed boundary conditions at the two ends of the graphene.[30,31] From Fourier's law, we define the thermal conductivity $\kappa$ as[32]

$$\kappa = \frac{J}{S\nabla T}, \tag{2}$$

where $\nabla T$ is the temperature gradient, $J$ is the heat flux from the heat source to sink, and $S$ is the cross-sectional area. To reach the non-equilibrium steady states, the system is relaxed for 50 ps under NVE ensemble. After that, 60 ps is used to calculate the thermal conductivity. The previous studies showed that using optimized Tersoff potential and LJ potential parameters can well describe the phonon properties and thermal transport behaviors in few-layer graphene, indicating that our calculated results are accurate and reliable.[33–35]

## 3. Results and discussion

We first consider perpendicular thermal transport in the T-FLGs of Fig. 1(c), where heat flux flows across three graphene layers along the perpendicular direction. The top and bottom layers are AA stacking, while the middle layer is rotated to tune the heat flux. Figure 2(a) presents thermal conductivity $\kappa_\perp$ as a function of rotation angle $\theta$. We find from Fig. 2(a) that $\kappa_\perp$ exhibits a non-monotonic dependence on $\theta$. When $\theta$ is changed from 0° to 60°, $\kappa_\perp$ first decreases gradually and then increases sharply. The lowest $\kappa_\perp$ occurs at $\theta = 30°$, which is a transition point. The thermal conductivity at $\theta = 30°$ is approximately $3.5\times10^{-3}$ W/mK, while those at $\theta = 0°$ and 60° are $4.3\times10^{-3}$ and 8.0 $\times10^{-3}$ W/mK. The latter are 1.3 and 2.3 times the former, respectively. All these values are small because of weak interlayer interactions between graphene layers. However, one can find that the perpendicular transport is sensitive to the stacking form and rotation angle.

In order to explain the effect of twist on the thermal transport, we compare the out-of-plane PDOSs of the three-layer graphene structures with $\theta = 0°$, 30°, and 60° as shown in Fig. 2(b). One can find that the PDOSs of the three structures exhibit different spectra, especially at the low phonon frequencies (< 10 THz). The PDOSs of $\theta = 60°$ and 30° present the highest and lowest values, respectively, while that of $\theta = 0°$ is in the middle. It is known that the out-of-plane phonon mode ZA of graphene is in a frequency range of 0–10 THz, and the perpendicular transport is strongly dependent on the ZA mode.[36–38] Therefore, the higher PDOS induces higher $\kappa_\perp$. In order to further explore the relation between interlayer interactions and rotation angle $\theta$, the interaction energies of the three structures are compared in Fig. 2(c). It is found that the interaction energy of $\theta = 60°$ is largest, while that of $\theta = 30°$ is the smallest. In the case of $\theta = 60°$, all layers are of AA stacking, and atoms between layers are directly stacked on each other. The shortest distance between atoms induces strong interlayer interaction. In the case of $\theta = 0°$, the stacking form between two nearest layers is AB, where only half of the atoms are directly stacked. In the case of $\theta = 30°$, the number of atoms having direct shortest-distance interactions is the smallest. Therefore, the interaction energy of $\theta = 60°$ is the largest, while that of $\theta = 30°$ is the smallest. The weaker interaction leads to weak coupling of out-of-plane phonon modes, and thus the thermal conductivity $\kappa_\perp$ is lower.

In Fig. 3, the effect of layer number on $\kappa_\perp$ of T-FLGs is calculated. The black, red, and blue lines in Fig. 3(a) present $\kappa_\perp$ values of T-FLGs with $\theta = 0°$, 30°, and 60° each as a function of the number of layers, respectively. It is found that all the thermal conductivities increase with layer number increasing gradually, and then converge to steady values after 13

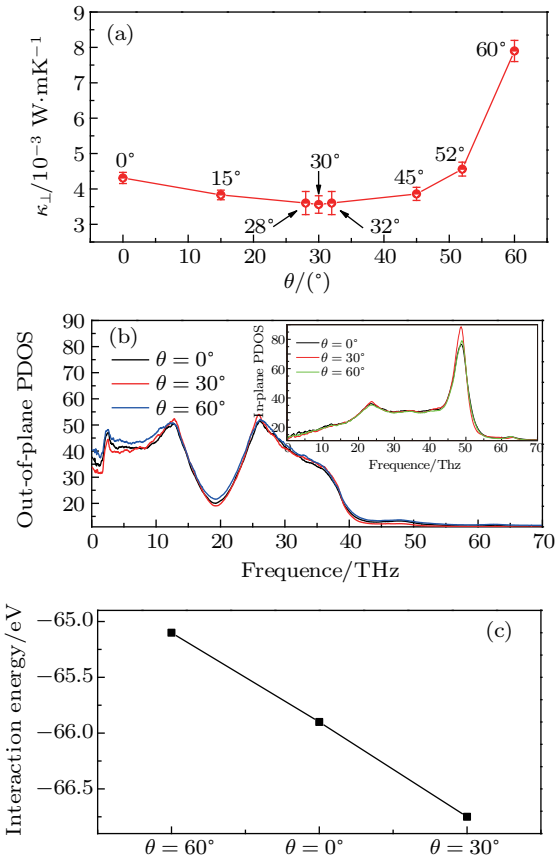



**Fig. 2.** (color online) (a) Perpendicular thermal conductivity $\kappa_\perp$ of T-FLG in Fig. 1(a) as a function of rotation angle $\theta$. (b) Comparison among out-of-plane PDOSs for three T-FLGs with $\theta = 0°$, 30°, and 60°. Inset shows the comparison among in-plane PDOSs for three T-FLGs with $\theta = 0°$, 30°, and 60°. (c) Comparison among interlayer interaction energies of the three T-FLGs.

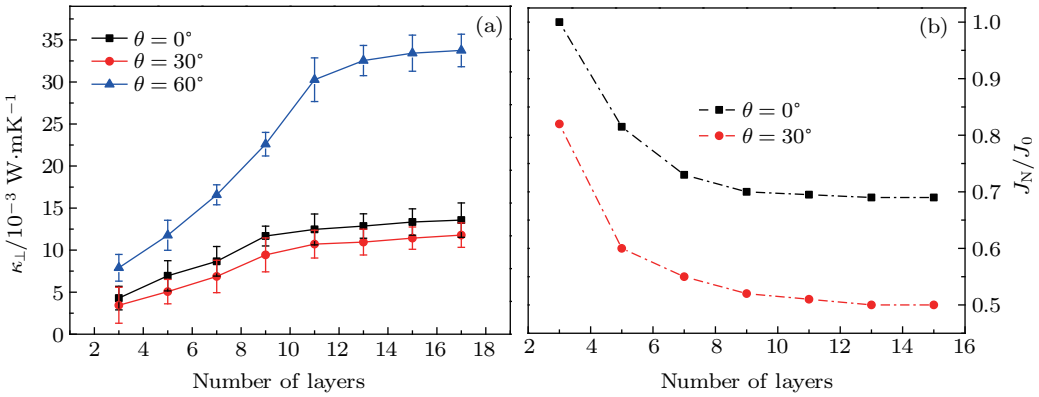



**Fig. 3.** (color online) (a) Plots of perpendicular thermal conductivity $\kappa_\perp$ of T-FLGs versus the number of layers. (b) The comparison between the values of normalized heat flux $J = J_N/J_0$ for T-FLGs with $\theta = 0°$ (black dash-dotted line) and 30° (red dash-dotted line), where $J_N$ is the heat flux of twisted $N$-layer structure and $J_0$ is the heat flux of three-layer graphene with $\theta = 0°$.

layers. This indicates that thermal transport in the few-layer structures approaches the transport in the bulk gradually after 13 layers. Relatively, the thermal conductivity of $\theta = 60°$ grows fast as the layer increases. The steady value is approximately $35.0\times10^{-3}$ W/mK, which is 3 times more than that of $\theta = 30°$ structure. The difference between the structures of $\theta = 0°$ and 30° seems small. To clearly compare the difference between $\theta = 0°$ and 30° structures, the values of normalized heat flux $J = J_N/J_0$ of the two structures each as a function of layer number are shown in Fig. 3(b). Here $J_N$ is the heat flux of twisted $N$-layer structure, while $J_0$ is the heat flux of three-layer graphene with $\theta = 0°$. The heat fluxes are calculated by setting heat baths separately on top and bottom layers, and temperature difference $\Delta T = 30$ K is fixed. With the increase of the layer number, the heat fluxes of $\theta = 0°$ and 30° both first drop and then converge gradually. One can note that the trend of heat fluxes in Fig. 3(b) is inverse to that of thermal conductivities in Fig. 3(a). This is because the decrease of temperature difference between layers is faster than the increase of thermal conductivities when the layer number is increased. One can clearly find that the heat flux in $\theta = 30°$ structure drops more rapidly than that in $\theta = 0°$ structure. From these results, one can conclude that the T-FLGs inherit the thermal transport characteristics of the three layer structures: the $\theta = 60°$ structure has the highest thermal transport ability while $\theta = 30°$ structure has the weakest ability. Because all the T-FLGs possess small thermal conductivities, i.e., high thermal resistances, these materials have great potential applications in thermal insulation.[39–41] One can tune the insulation effect by rotating the angle between layers. Obviously, the structure with $\theta = 30°$ exhibits the best insulation effect.

Next, we consider parallel thermal transport in T-FLGs where heat flux flows in the structure along the parallel direction. In Fig. 4(a), we calculate the values of parallel thermal conductivity $\kappa_\parallel$ of twisted two-layer graphene in Fig. 1(b) with different values of rotation angle $\theta$. One can find that, the relation between thermal conductivity and rotation angle is completely different from that in the case of perpendicular transport. Here, $\kappa_\parallel$ of $\theta = 30°$ has the highest value, while those of $\theta = 0°$ and 60° are smaller. The parallel transport is related to two processes: one is the transport in the graphene layers, the other is the phonon scattering between layers because of the interlayer coupling. Because the layer coupling is relatively weak, the direct effect of interlayer interaction on the parallel transport is very limited. This can be illustrated by comparing the in-plane PDOSs of three structures, which is shown in the inset of Fig. 2(b). Therefore, the parallel transport is dominated by the edges of graphene layers. For the $\theta = 30°$ structure, along the transport direction, the two graphene layers have zigzag and armchair edges, respectively. For the $\theta = 0°$ and 60° structures, both layers have the armchair edges here. The thermal conductivity of zigzag nanoribbon is larger than that of armchair nanoribbon because of anisotropic transport in graphene.[42,43] Therefore, the $\kappa_\parallel$ value of $\theta = 30°$ is larger than those of $\theta = 0°$ and 60°. To describe the effect of interlayer scattering on the thermal transport, in Fig. 4(a) the $\kappa_\parallel$ values of the structures without interlayer coupling are also presented for comparison, and the difference $\Delta\kappa_\parallel$ between the structures with and without coupling is shown in Fig. 4(b). It is seen from Fig. 4(b) that the difference of thermal conductivity is sensitive to the rotate angle, and exhibits a somewhat similar trend to that of the $\kappa_\perp$ in Fig. 2(a). This indicates that the interlayer scattering in the $\theta = 30°$ structure is the smallest because of the weak interlayer interaction mentioned above. Therefore, the strength of interlayer coupling has an inverse effect on the perpendicular transport compared with that on the parallel transport. It is conducible to the perpendicular transport while suppressing the parallel transport.

In Fig. 4(c), we calculate $\kappa_\parallel$ values of three T-FLGs ($\theta = 0°$, 30°, and 60°) varying with layer number. All $\kappa_\parallel$ values decrease rather than increase with layer number increasing, which is inverse to the trend in Fig. 3(a). This is

because more graphene layers strengthen phonon scattering and thus weaken the thermal transport along the parallel direction. With the increase of layer number, the interlayer scattering becomes steady gradually and then the thermal conductivities converge. To compare the interlayer scatterings in the three structures, we calculate the difference $\Delta\kappa_{\parallel}$ between the cases with and without interlayer coupling in these structures as shown in Fig. 4(d). The $\Delta\kappa_{\parallel}$ of $\theta = 60^{\circ}$ increases rapidly with the increase of layer number, while that of $\theta = 30^{\circ}$ increases slowly. This further proves that the $\theta = 30^{\circ}$ structure has the weakest interlayer interaction. Li *et al.* investigated experimentally the thermal conductivity of suspended twisted bilayer graphene by using an optothermal Raman technique, and they found that the thermal conductivity of twisted bilayer graphene is lower than those of monolayer graphene and AB stacked bilayer graphene in the entire temperature range examined (∼ 300–700 K).[44] These are consistent with our results.

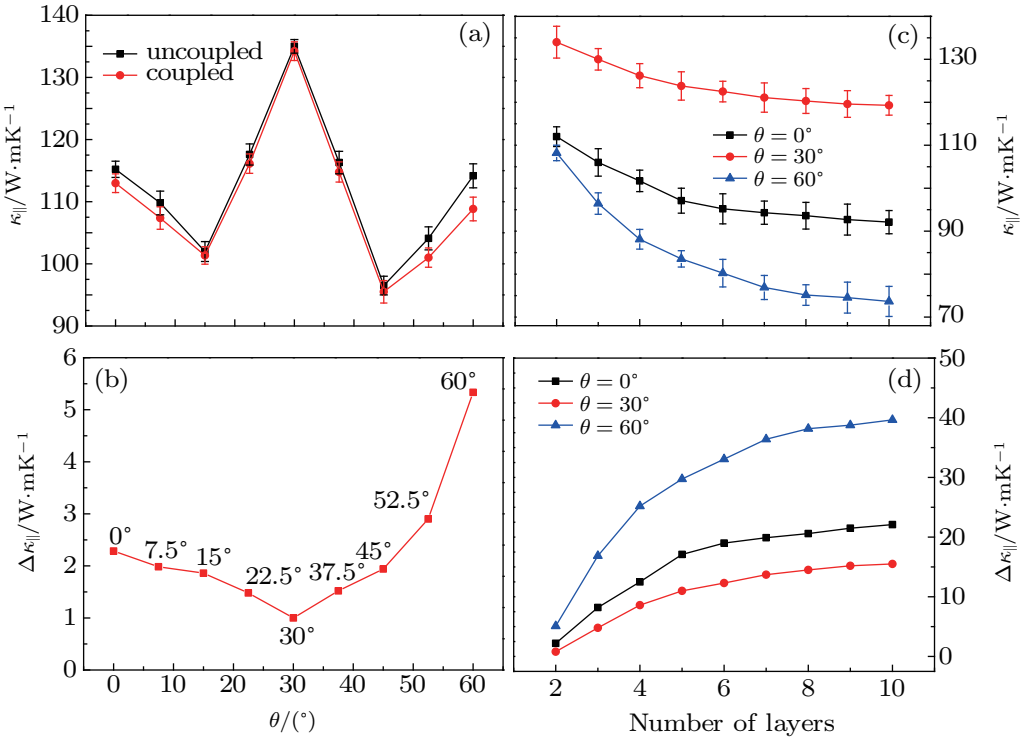



**Fig. 4.** (color online) (a) Parallel thermal conductivity $\kappa_{\parallel}$ of twisted bilayer graphene in Fig. 1(b) as a function of rotation angle $\theta$, where the black and red lines represent the cases with and without interlayer coupling. (b) Difference between thermal conductivities $\Delta\kappa_{\parallel}$ ($= \kappa_{\parallel}$ without coupling $-\kappa_{\parallel}$ with coupling) varying with rotation angle $\theta$. (c) Variations of $\kappa_{\parallel}$ of T-FLGs with $\theta = 0^{\circ}$, $30^{\circ}$, and $60^{\circ}$ with the number of layers. (d) The values of $\Delta\kappa_{\parallel}$ of T-FLGs with the number of layers.

## 4. Conclusions

In this work, we study perpendicular and parallel thermal transports in the T-FLGs, by using MD simulations. The effect of twist on the thermal transport is discussed by comparing the thermal conductivities $\kappa_{\perp}$ and $\kappa_{\parallel}$ in the T-FLGs with different values of rotation angle $\theta$. When $\theta$ is changed from $0^{\circ}$ to $60^{\circ}$, $\kappa_{\perp}$ first decreases and then increases, where $\theta = 30^{\circ}$ is the transition point. This indicates that T-FLG with $\theta = 30^{\circ}$ has the strongest interlayer coupling, which is proven by analyzing PDOS and interlayer interaction energy. For the parallel transport, the relation between thermal conductivities $\kappa_{\parallel}$ and $\theta$ is complicated, because intra-layer thermal transport is more sensitive to the edge of the layer than their stacking form. However, the dependence of interlayer scattering on $\theta$ is similar to that on the $\kappa_{\parallel}$, which reveals the inverse effect of interlayer coupling on perpendicular and parallel transports. The increase of layer number further increases the twist effect in the T-FLG. These results provide an insight into understanding thermal transports in two-dimensional VDWs materials.

## References

[1] Novoselov K S, Geim A K, Morozov S V, Jiang D, Zhang Y, Dubonos S V, Grigorieva I V and Firsov A A 2004 *Science* **306** 666
[2] Neto A C, Guinea F, Peres N M, Novoselov K S and Geim A K 2009 *Rev. Mod. Phys.* **81** 109
[3] Chen Y P, Xie Y E, Sun L and Zhong J 2008 *Appl. Phys. Lett.* **93** 092104
[4] Zhang Y, Tan Y W, Stormer H L and Kim P 2005 *Nature* **438** 201
[5] Balandin A A, Ghosh S, Bao W, Calizo I, Teweldebrhan D, Miao F and Lau C N 2008 *Nano Lett.* **8** 902
[6] Evans W J, Hu L and Keblinski P 2010 *Appl. Phys. Lett.* **96** 203112
[7] Ghosh S, Calizo I, Teweldebrhan D, Pokatilov E P, Nika D L, Balandin A A, Bao W, Miao F and Lau C N 2008 *Appl. Phys. Lett.* **92** 151911
[8] Wassmann T, Seitsonen A P, Saitta A M, Lazzeri M and Mauri F 2008 *Phys. Rev. Lett.* **101** 096402
[9] Wang X, Zhou X, Yao K, Zhang J and Liu Z 2011 *Carbon* **49** 133
[10] Brown L, Hovden R, Huang P, Wojcik M, Muller D A and Park J 2012 *Nano Lett.* **12** 1609
[11] Carozo V, Almeida C M, Ferreira E H, Cancado L G, Achete C A and Jorio A 2011 *Nano Lett.* **11** 4527

[12] Ping J and Fuhrer M S 2012 *Nano Lett.* **12** 4635

[13] Hass J, Varchon F, Millan-Otoya J E, Sprinkle M, Sharma N, de Heer W A, Berger C, First P N, Magaud L and Conrad E H 2008 *Phys. Rev. Lett.* **100** 125504

[14] Luican A, Li G, Reina A, Kong J, Nair R, Novoselov K S, Geim A K and Andrei E 2011 *Phys. Rev. Lett.* **106** 126802

[15] Havener R W, Zhuang H, Brown L, Hennig R G and Park J 2012 *Nano Lett.* **12** 3162

[16] Bistritzer R and MacDonald A H 2011 *Proceedings of the National Academy of Sciences* **108** 12233

[17] Li G, Luican A, Dos Santos J L, Neto A C, Reina A, Kong J and Andrei E 2010 *Nat. Phys.* **6** 109

[18] Dos Santos J L, Peres N and Neto A C 2007 *Phys. Rev. Lett.* **99** 256802

[19] Gupta A K, Tang Y, Crespi V H and Eklund P C 2010 *Phys. Rev. B* **82** 241406

[20] Righi A, Costa S, Chacham H, Fantini C, Venezuela P, Magnuson C, Colombo L, Bacsa W, Ruoff R and Pimenta M 2011 *Phys. Rev. B* **84** 241409

[21] Cocemasov A I, Nika D L and Balandin A A 2013 *Phys. Rev. B* **88** 035428

[22] Nika D L, Cocemasov A I and Balandin A A 2014 *Appl. Phys. Lett.* **105** 031904

[23] Plimpton S, Crozier P and Thompson A 2007 *Sandia National Laboratories* **18**

[24] FrantzDale B, Plimpton S J and Shephard M S 2010 *Engineering with Computers* **26** 205

[25] Powell D, Migliorato M and Cullis A 2007 *Phys. Rev. B* **75** 115202

[26] Lindsay L and Broido D 2010 *Phys. Rev. B* **81** 205441

[27] Heinz H, Vaia R, Farmer B and Naik R 2008 *The Journal of Physical Chemistry C* **112** 17281

[28] Galliéro G, Boned C, Baylaucq A and Montel F 2006 *Phys. Rev. E* **73** 061201

[29] Petculescu A G and Lueptow R M 2005 *The Journal of the Acoustical Society of America* **117** 175

[30] Hu J, Ruan X and Chen Y P 2009 *Nano Lett.* **9** 2730

[31] Zhong W R, Huang W H, Deng X R and Ai B Q 2011 *Appl. Phys. Lett.* **99** 193104

[32] Bernardin C and Olla S 2005 *J. Stat. Phys.* **121** 271

[33] Cao H Y, Guo Z X, Xiang H and Gong X G 2012 *Phys. Lett. A* **376** 525

[34] Lindsay L, Broido D and Mingo N 2011 *Phys. Rev. B* **83** 235428

[35] Singh D, Murthy J Y and Fisher T S 2011 *J. Appl. Phys.* **110** 044317

[36] Nika D L and Balandin A A 2012 *Journal of Physics: Condensed Matter* **24** 233203

[37] He R, Chung T F, Delaney C, Keiser C, Jauregui L A, Shand P M, Chancey C, Wang Y, Bao J and Chen Y P 2013 arXiv:1307.5914

[38] Wang Z, Xie R, Bui C T, Liu D, Ni X, Li B and Thong J T 2010 *Nano Lett.* **11** 113

[39] Wicklein B, Kocjan A, Salazar-Alvarez G, Carosio F, Camino G, Antonietti M and Bergström L 2015 *Nature Nanotechnology* **10** 277

[40] Shahil K M and Balandin A A 2012 *Solid State Commun.* **152** 1331

[41] Papadopoulos A M 2005 *Energy and Buildings* **37** 77

[42] Aksamija Z and Knezevic I 2011 *Appl. Phys. Lett.* **98** 141919

[43] Odaka S, Miyazaki H, Li S L, Kanda A, Morita K, Tanaka S, Miyata Y, Kataura H, Tsukagoshi K and Aoyagi Y 2010 *Appl. Phys. Lett.* **96** 062111

[44] Li H, Ying H, Chen X, Nika D L, Cocemasov A I, Cai W, Balandin A A and Chen S 2014 *Nanoscale* **6** 13402